Journal of Fluorescence (2019) 29:1291–1300
https://doi.org/10.1007/s10895-019-02452-7

ORIGINAL ARTICLE

Fluorescent N/Al Co-Doped Carbon Dots from Cellulose Biomass for Sensitive Detection of Manganese (VII)

Supuli Jayaweera[1,2] · Ke Yin[3] · Xiao Hu[4,5] · Wun Jern Ng[6]

Received: 28 July 2019 / Accepted: 1 October 2019 / Published online: 9 November 2019

Abstract

Development of metallic and nonmetallic heteroatom doped carbon dots have gained attention due to their enhanced physicochemical and photoluminescence properties. In this study, a facile one pot hydrothermal carbonisation approach was taken to synthesise nitrogen, aluminum co-doped carbon dots (N/Al-CDs) with a photoluminescence quantum yield of 28.7%. Durian shell, a cellulose biomass waste, was used as the primary carbon source and compared to previously reported cellulose based carbon dots, this study presents one of the highest quantum yields. The structural and fluorescent properties of the synthesised N/Al-CDs were characterized through X-ray photoelectron spectroscopy (XPS), fluorescence spectra, and Fourier transform infrared spectroscopy (FTIR). The maximum emission was at 415 nm upon excitation at 345 nm. The synthesised N/Al-CDs were resistant to photobleaching and highly photostable within the pH, ionic strength and temperature variations investigated. The transmission electron microscopy (TEM) images showed particles were quasi-spherical and well dispersed with an average diameter of 10.0 nm. Further, the N/Al-CDs was developed as a fluorescence sensor for highly selective and sensitive detection of Mn (VII) ions. A linear relationship was developed over a concentration range of 0–100 μM while the limit of detection was 46.8 nM. Application of the sensor for detection of Manganese (VII) to two real water samples showed relative standard deviation was less than 3.9% and 1.3%, respectively.

Keywords Carbon dots · Durian shell waste · Nitrogen aluminum doping · Fluorescence · Mn^{7+} detection

Introduction

Zero-dimensional Carbon nanodots (CDs) is an emerging member to the functional nanomaterial family and it has drawn attention due to its low cytotoxicity, tunable photoluminescence, chemical inertness, biocompatibility, and resistance to photobleaching [1, 2]. Consequently, carbon dots have a wide spectrum of potential applications such as environmental monitoring, photocatalysis, bioimaging, and energy storage [3–6]. Photoluminescence (PL) is a key characteristic of CDs and developments have been made to increase PL by size control, surface functionalization/ passivation, and heteroatoms doping [7, 8]. Due to the facile synthesis process and the high tunability of the CDs, heteroatoms doping with one or a combination of nitrogen, sulfur, boron and phosphorous doping agents is a common synthesis method in CD production [9–11]. Introduction of atomic dopants generated n-type or p-type carriers which changed the electronic and optical properties associated with the HOMO-LUMO energy gap [12]. Thus, controlled doping can greatly enhance the quantum yield. Recently metal dopants have been used for CD production with Cu-CDs produced with sodium citrate and cuprous chloride for Fe^{3+} sensing [13], Zn-CDs produced with sodium citrate and zinc chloride for glucose [14], and cholesterol and xanthine sensing using N-Cu CDs produced by hydrothermal reaction between citric acid, and copper acetate [15], and Mn coordinated CDs for cell imaging [16]. Compared to the non-metals, the use of metals increased the

✉ Wun Jern Ng
WJNg@ntu.edu.sg

1 Nanyang Environment & Water Research Institute, Interdisciplinary Graduate School, Nanyang Technological University, Singapore, Singapore

2 Residues & Resource Reclamation Centre, Nanyang Environment & Water Research Institute, Nanyang Technological University, Singapore, Singapore

3 Department of Environmental Engineering, School of Biology and the Environment, Nanjing Forestry University, Nanjing, China

4 School of Materials Science and Engineering, Nanyang Technological University, Singapore, Singapore

5 Environmental Chemistry and Materials Centre, Nanyang Environment & Water Research Institute, Nanyang Technological University, Singapore, Singapore

6 Environmental Bio-innovations Group (EBiG), School of Civil and Environmental Engineering, Nanyang Technological University, Singapore, Singapore

electron density in CDs which then increased the electronic transitions for improved optical properties [17]. Further, introducing metals to the carbon matrix elevated electronic mobility to improve the physiochemical properties of CDs [14, 17].

More than 80% of the Mn^{7+} ion used in the drinking water treatment industry is to remove dissolved iron and manganese, hydrogen sulfide and control taste and odour [18]. It is also used as a bleaching agent, treatment of sewage sludge, and as a biocide to control fungi and algae [18–20]. However, such usage can lead to Mn^{7+} residuals – e.g. in the drinking water after filtration which can lead to discoloration and metallic taste, skin irritation and gastrointestinal distress [18]. Given the recurrent usage, various techniques have been developed to detect Mn^{7+} over the years. These methods are primarily based on titration with high purity chemicals like sodium thiosulfate/iodide and sodium oxalates in the presence of strong acids [21, 22]. Apart from harmful chemicals, these methods are time consuming and the accuracy of the results are highly sensitive to the environmental conditions (e.g. pH, temperature) [23]. Thus, there is a requirement for fast and reliable detection methods for Mn^{7+} and CDs are an emerging nanomaterial that has shown a potential to sense a broad range of analytes including cations, anions, organic molecules and biological compounds [24]. The unique optical characteristics of CDs have enabled to detect analytes cheaply, efficiently and accurately even at low concentrations [25].

In this study, durian shell waste (DSW) together with urea and aluminum nitrate were used for the first time in a facile hydrothermal reaction to produce N/Al-CDs. DSW primarily consists of cellulose along with other oxygen/nitrogen containing compounds including carboxylic acids, phenols, esters and amino acids [26]. It is reported that aluminum has high affinity with oxygen functional groups to form stable chelator complex [27] and given DSW is a rich source for oxygenated groups, it provides anchoring sites for aluminum to incorporate into the carbon structure through oxygen groups and thereby increase the doping efficiency leading to high photoluminescence (PL) [28, 29]. The synthesised N/Al-CDs were highly fluorescent with a quantum yield (QY) of 28.7% whilst the QY of metal free N-CDs was only 10.4%. PL of the N-Al co-doped DSW based CDs was much higher than values previously reported for cellulose based CDs where the QYs were 7.6% for corn stalks [30], 6.9% for pomelo peels [31] and 9.2% for wheat straw [32]. The values in this study are comparable with Zn doped sodium citrate CDs and Gd-ethanediamine doped citrate acid which had QYs of 32.3% and 21%, respectively [14, 33]. Considering the low PL typically shown by cellulose based CDs, the proposed method suggested a potentially viable avenue to develop future cellulose CDs.

This paper reports a facile one-step hydrothermal carbonisation method to synthesize highly fluorescent carbon dots from DSW by co-doping with an aluminum-nitrogen mix. The N/Al-CDs were characterised structurally and optically to assess the presence of dopants and their impact on the quality of carbon dots. Finally, the N/Al-CDs were used to develop a ratiometric sensor with a linear relationship with Mn^{7+} concentration. This relationship was verified using real water samples.

Experimental Section

Materials

DSW was obtained and powdered according to ref. [26]. Urea, $LaCl_3.7H_2O$, NaOH and NaCl were obtained from Merck Pte. Ltd., US. $KMnO_4$, $Al(NO_3)_3{\cdot}9H_2O$, $CoCl_2{\cdot}6H_2O$, $CrCl_3{\cdot}6H_2O$, $Pb(NO_3)_2$, $ZnCl_2$, $CuCl_2{\cdot}2H_2O$, $Ce(NO_3)_3{\cdot}6H_2O$, $K_2Cr_2O_7$, $FeCl_3{\cdot}6H_2O$ were obtained from Sigma-Aldrich Co. LLC, US. Quinine sulfate and $Ni(NO_3)_2{\cdot}6H_2O$ were purchased from Alfa Aesar, US. $MgCl_2{\cdot}6H_2O$, $CaCl_2{\cdot}2H_2O$ and $FeCl_2{\cdot}6H_2O$ were purchased from Sinopharm Chemical Reagent Co. Ltd., China. All the chemicals were of analytical grade and used as received without further purification.

Synthesis of N/Al-CDs

N/Al-CDs were synthesised by mixing finely ground DSW (1 g) powder (0.22 mm mesh) with a 0.1 g Urea and 0.1 g of Aluminum nitrate. The mixture was then placed in a 45 ml Teflon-lined stainless steel autoclave reactor with 25 ml of deionized (DI) water. The sealed reactor was then heated at 210 °C for 12 h. After the mixture was cooled to room temperature, the CD particles were separated and purified according to method described in Jayaweera et al. [5]. For comparison, N-CDs were prepared via the same method except for the addition of Aluminum nitrate.

Characterisation

Fourier transform infrared spectroscopy (FTIR) was performed with a Bruker Tensor 27 FTIR spectrophotometer. Elemental mappings of CDs were done with a JEOL JSM 7200F field emission scanning electron microscope (FE-SEM). Morphology and the crystalline structures of CDs were viewed on a JEOL 2010 transmission electron microscope (TEM) under 200 kV. Kratos Analytical AXIS Supra photoelectron spectrometer was used for X-ray photoelectron spectroscopy (XPS) measurements. Fluorescence spectral measurements were performed on an Agilent Cary Eclipse Fluorescence Spectrophotometer. Fluorescent decay curves were obtained from a Horiba fluorolog3 spectrofluorometer equipped with a 360 nm nanoLED. Ultraviolet-Visible (UV-

Vis) absorption spectra were determined with an Agilent Varian Cary 50 UV/Vis Spectrophotometer.

Quantum Yield (QY) Measurements

The QY of the CDs were determined using the relative QY method with quinine sulfate in 0.5 M H_2SO_4 (QY = 54%) as the reference. Five solutions with different CD concentrations were prepared with absorbance less than 0.05 to minimize reabsorption. A graph was plotted relating the integrated PL intensity at an excitation wavelength of 345 nm with the absorbance to determine the final QY according to the following equation [5].

$$QY_{CD} = QY_{st}\left(\frac{I_{CD}}{I_{st}}\right)\left(\frac{A_{st}}{A_{CD}}\right)\left(\frac{\eta_{CD}}{\eta_{st}}\right)^2$$

where subscripts "CD" and "st" stands for CDs and reference standards, respectively. "I" refers to the integrated Photoluminescence (PL) intensity, "A" refers to the absorbance measured at the excitation wavelength and "η" refers to the refractive index.

Detection of Mn^{7+}

The sensitivity of Mn^{7+} ions was determined by mixing 60 μL of CD solution (125 μg/ml) with the various Mn^{7+} ion solutions with concentrations from 0 to 180 μM to reach a total volume of 2 ml. Each assay was mixed thoroughly and kept for 15mins at room temperature before recording the PL intensity at an excitation wavelength of 345 nm. Selectivity tests were conducted with Ca^{2+}, Cr^{3+}, Ni^{2+}, La^{3+}, Fe^{2+}, Fe^{3+}, Ce^{3+}, Cr^{6+}, Pb^{2+}, Na^{+}, Mg^{2+}, Zn^{2+}, Cu^{2+} and Co^{2+} ions with a metal ion concentration of 100 μM. All measurements were performed in triplicates.

Results and Discussion

Characterisation of N-Al CDs

Functional groups on the surface of N/Al-CDs and N-CDs were characterized with ATR-FTIR as shown in Fig. 1a. The broad absorption peak at 3310 cm^{-1} corresponded to the phenolic-OH and N-H stretching vibrations [5]. The absorption peak at 2960 cm^{-1} and 1380 cm^{-1} were ascribed to the C-H stretching and bending vibrations, respectively [34]. Peaks at 1600 cm^{-1} and 1450 cm^{-1} corresponded to the sp^2 C = C bending and sp^3 CH_2 bands, respectively [30]. The vibration band at 1050 cm^{-1} in the N-CDs corresponded with the C–O bond [35]. The affinity of Al to bond with oxygen functional groups was further corroborated when the presence of aluminum on the N/Al-CDs was confirmed by the bands at 1070 cm^{-1} and 740 cm^{-1} which were ascribed to the Al-O-H and Al-O bonds, respectively [36]. These hydroxyl and nitrogen functional groups increased hydrophilicity and thus improved the solubility of N/Al-CDs in water [37]. Raman spectroscopy (Fig. 1b) indicated two vibrational peaks, at 1360 cm^{-1} and 1580 cm^{-1}, and these were attributed to the disorderly network of sp^2 carbon clusters (D) and graphitic (G) bands, respectively [38, 39]. The spectrum was fitted with a double Gaussian function and the integrated areas of the respective curves were used to calculate an I_D/I_G ratio of 1.22. This suggested the synthesised N/Al-CDs had high surface defects compared to the sp^2 hybridized graphene structure.

Morphology and structural analysis of the CDs was performed with TEM imaging as shown in Fig. 1c. The N/Al-CDs were quasi-spherical and well separated indicating an even aqueous distribution of CD particles in the solution. The inset on Fig. 1c shows a structured crystallinity with a lattice spacing of 0.24 nm correlated to (100) the in-plane graphene structure [40]. The diameters of CDs ranged from 6 to 14 nm with an average particle size of 10 nm (Fig. 1d). EDS elemental mapping distribution of carbon, oxygen, nitrogen and aluminum (Fig. 2) further indicated the elements were evenly distributed on the CD surface.

Elemental composition of the CDs was analysed by XPS and full scan spectrum (Fig. 3a) showed four dominant peaks attributed to C1s (79.05%), O1s (16.58%), N1 s (2.71%) and Al 2p (1.66%) indicating successful integration of aluminum and nitrogen to the CDs. The high resolution C1S spectrum (Fig. 3b) indicated three binding energies at 284.8, 285.78 and 288.3 eV. This corresponded to the C-C/C-H, C-O/C-N, and C=ONH/C=OO- bonds, respectively [41, 42]. The N1 s spectrum (Fig. 3c) showed three peaks at 395.9, 397.5 and 399.1 eV which were attributed to the N-O, Al-N and Pyridine N bonds, respectively [43, 44]. The binding energy spectrum of Al 2p showed (Fig. 3d) three peaks at 73.2, 73.8 and 74.4 eV which corresponded to Al-N, Al-O and Al-OH, respectively [45, 46]. These results are further corroborating the FTIR results and indicate that the Al^{3+} had coordinated with oxygen and nitrogen groups.

Optical Properties of N-Al CDs

The optical properties of the N/Al-CDs were investigated with UV-vis absorption and fluorescence analysis. The UV absorption spectra (Fig. 4a) showed a strong peak at 264 nm and a weak peak at 305 nm. The former peak corresponded with the π-π* transitions of aromatic sp^2 domains [47] while the weak peak at 314 nm corresponded with the n– π* transition of the C=O/C=N groups [48]. As shown in Fig. 4a inset, the N/Al-CDs emitted a bright blue fluorescence under a 365 nm UV light which is attributed to the intrinsic near band edge electron hole recombination in the sp^2 cluster [15]. Further, the

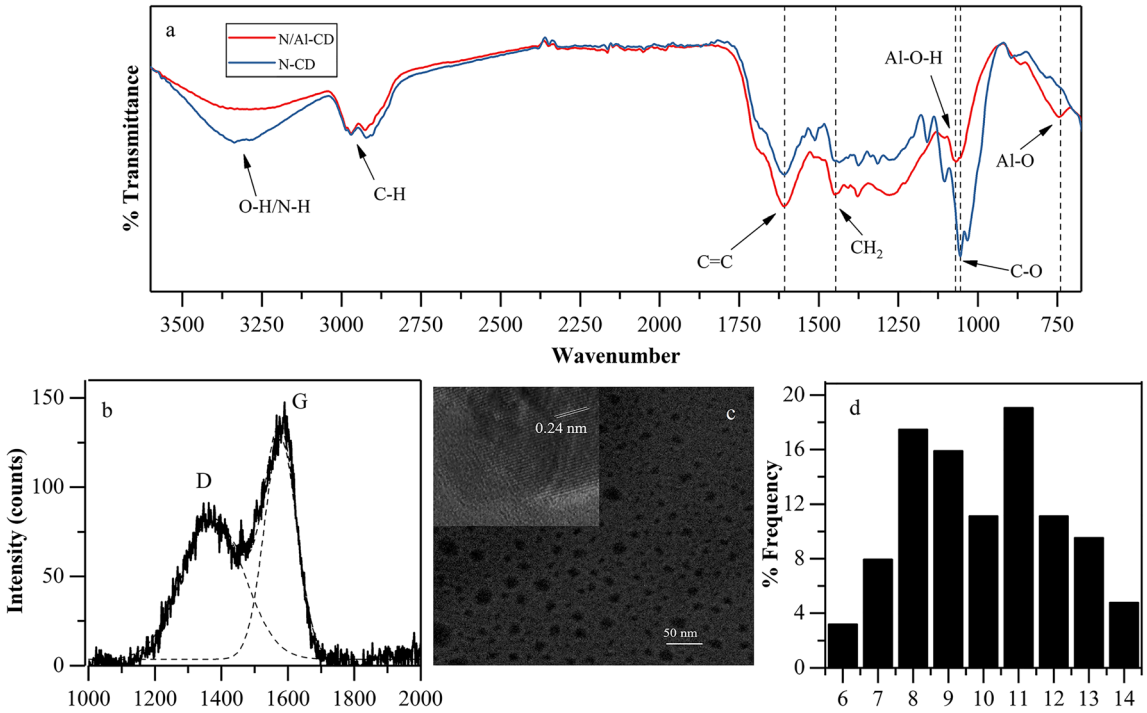

Fig. 1 **a** FTIR Spectra of N-Cd and N/Al-CDs, **b** Raman Spectra N/Al-CDs, **c** TEM and the HRTEM (inset) images, **d** Particle diameter distribution histogram of N/Al-CDs

maximum photoluminescence was observed at 415 nm upon excitation at 345 nm.

Figure 4b presents the fluorescence emission spectra of N/Al-CDs at different excitation wavelengths. Two distinctive regions could be observed where excitation independent emission was observed from the 300–345 nm excitation and an excitation dependent emission from 350 to 420 nm excitation. Several mechanisms have been proposed to explain CDs emission but the exact mechanism is yet to be confirmed [49]. Based on the literature, the emission of N/Al-CDs could be due to the combined effects of emissions resulting from the π-π^* transitions of the sp^2 clusters and the surface functional

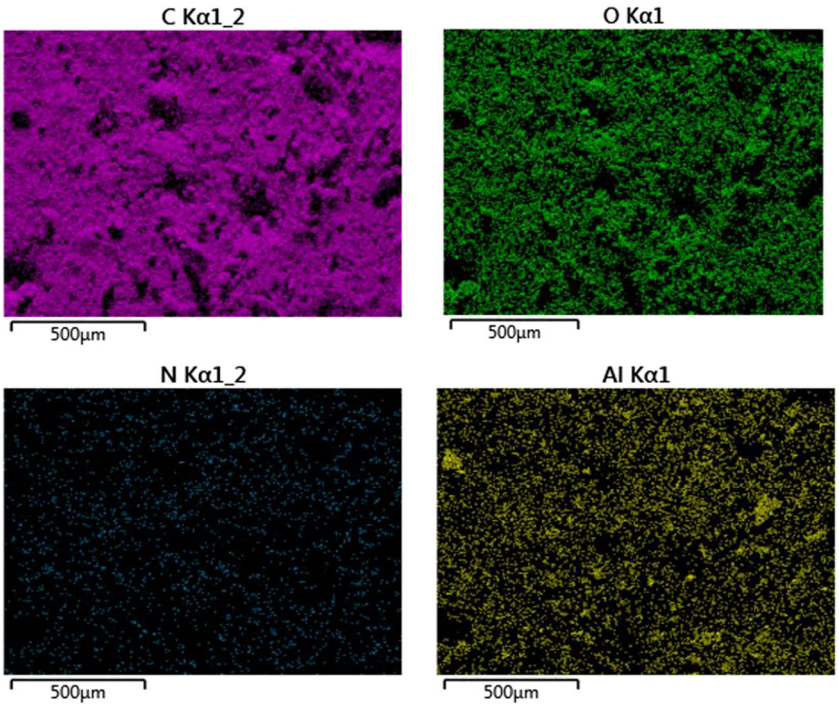

Fig. 2 Elemental mapping of CDs showing carbon (purple), oxygen (green) nitrogen (blue) and aluminum (yellow)

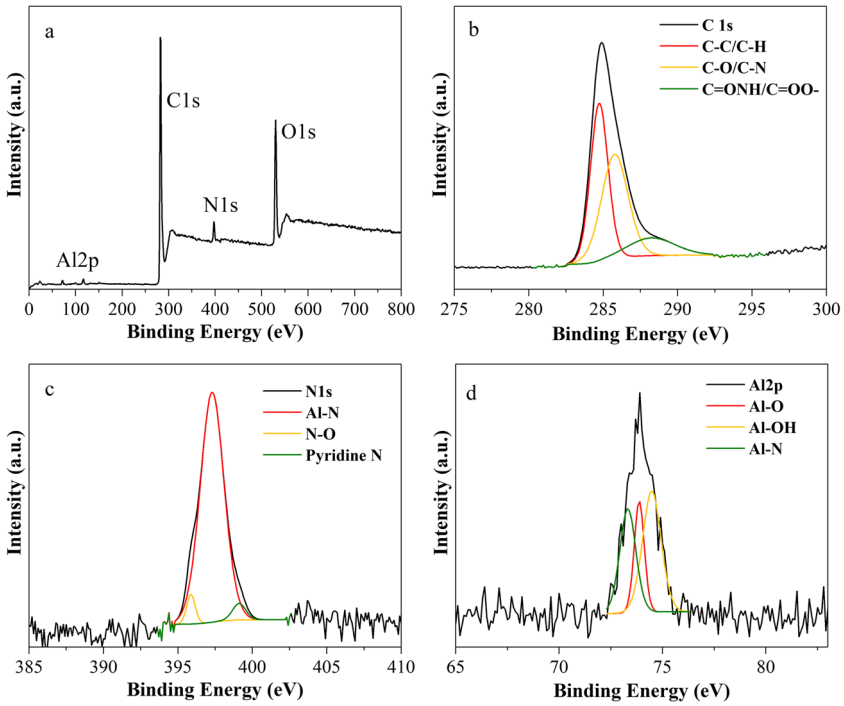

Fig. 3 **a** XPS spectrum of the N/Al-CDs with High-resolution, **b** C1s, **c** N1 s, **d** Al 2p (f) spectra

groups [15, 49]. The initial excitation independent emission was primarily governed by the single recombination of electron-hole pairs in the sp^2 cluster. However, at higher wavelengths, the energy would be insufficient to excite these sp^2 clusters and the emission of N/Al-CDs would then have been dominated by the surface trapping states which introduced new energy band gaps on the N/Al-CDs resulting in excitation dependent emission after 350 nm [15, 50]. In addition to the fluorescence spectrum, the stability of the N/Al-CDs was investigated by measuring the variation of PL intensity against pH, temperature, ionic strength and photobleaching. The variation is interpreted by the mean normalized intensity (MNI) and the relative standard deviation (RSD). N/Al-CDs showed high stability under varying pH level from 3 to 11 (Fig. 5a) with an MNI of 0.989 and an RSD of 2.17%. The PL change with ionic strength was measured by exposing the synthesised CDs to increasing concentrations of NaCl solutions up to 500 mM (Fig. 5b). N/Al-CDs exhibited high resistance to the ionic strength with an MNI of 0.96 and an RSD of 3.02%. Similarly, the resilience of CDs to temperature variation was also high (Fig. 5c) with an MNI of 0.97 and an RSD of 3.54%. Despite the stability, PL intensity decreased slightly with increasing temperature. This could be attributed to thermal activation of non-radiative trappings in surface and defective sites [5, 51]. Finally, the photostability was measured by continuous exposure to UV irradiation by a Hg lamp (Fig. 5d). PL intensity of N/Al-CDs only reduced by 8% and 14% after continuous exposure of up to 60 mins and 120 mins, respectively, indicating high resistance to photobleaching [52]. Thus, it can be concluded that the

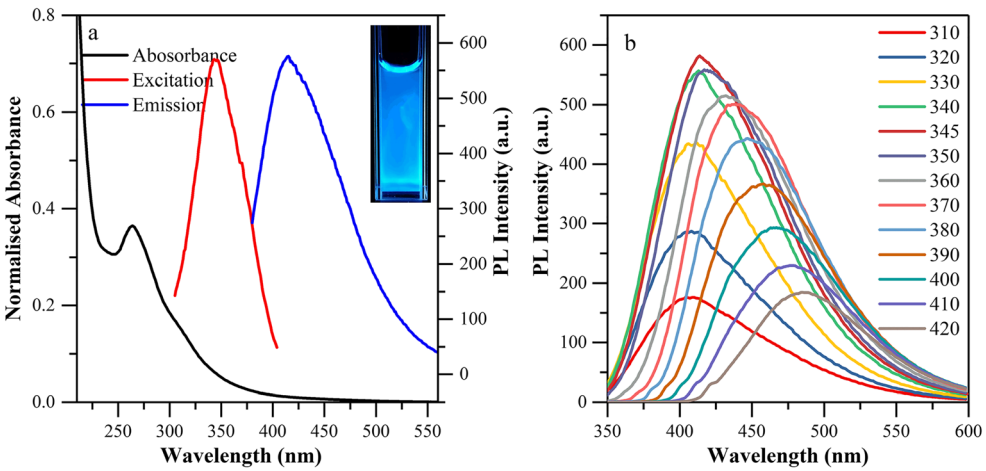

Fig. 4 **a** Absorption spectrum with maximum excitation and emission spectra and a photograph of N/Al-CDs under 365 nm UV light (inset), **b** PL emission spectra of N/Al-CDs at different excitation wavelengths

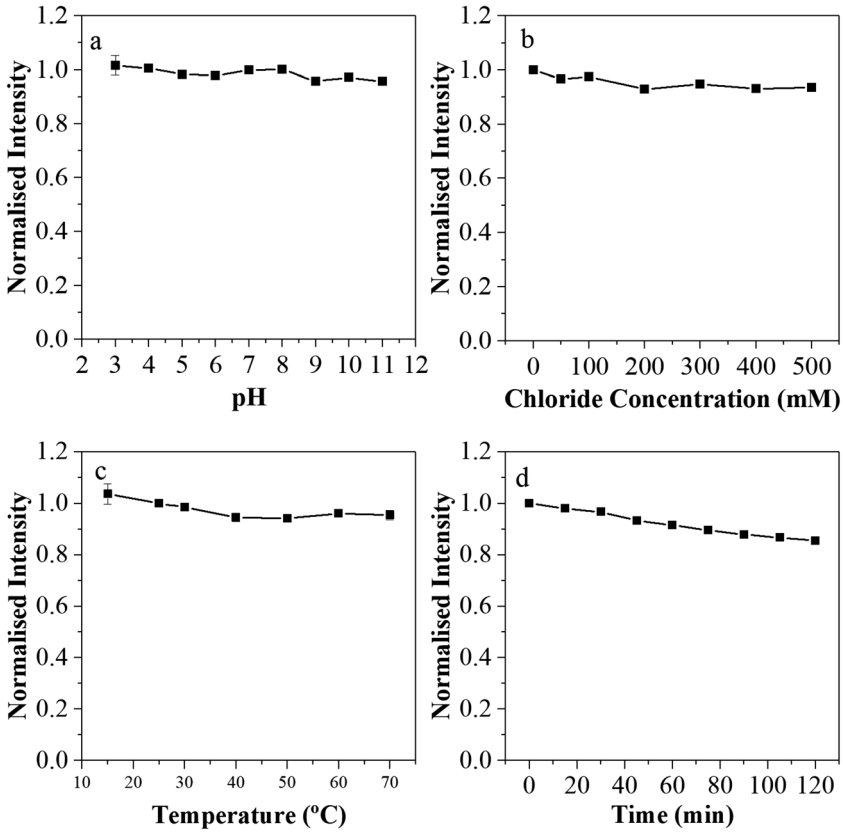

Fig. 5 **a** Effect of pH, **b** Effect of chloride concentration, **c** effect of temperature, **d** photostability under continuous UV irradiation on the PL intensity of N/Al-CDs measured at 345 nm excitation

synthesised N/Al-CDs had positive fluorescent properties with good optical stability.

Detection of Mn (VII)

In this study, the excellent water solubility and the optical stable characteristics of N/Al-CDs were used to detect dissolved Mn^{7+} concentrations in water to develop a sensitive and selective fluorescent nano-probe. The selectivity of N/Al-CDs towards sensing Mn^{7+} was investigated by comparing the effects on fluorescence in the presence of different metal ions (Fig. 6a). N/Al-CDs fluorescence was quenched nearly 85% with the introduction of Mn^{7+} whereas the intensity of other metals except Fe^{3+} and Cr^{6+} was only affected by ±5%. The Cr^{6+} ion quenched 40% of the fluorescence. This was due to inner filter effects which will be discussed later in this section. In a previous report, undoped DSW based CDs showed high selectivity towards Fe^{3+}. This was ascribed to Fe^{3+} complex formation with oxygen rich CD surface [26]. However, the introduction of N-Al doping mix has reduced the quenching effect to 20% and this was attributed to the formation of Al-O bonds that subsequently reduced the Fe^{3+} ground state complex formation with oxygen groups. Thus, N/Al-CDs has better selectivity towards Mn^{7+} ion. To further quantify the fluorescence quenching, measurements were taken for a series of Mn^{7+} concentration from 0 to 180 μM (Fig. 6b). Quenching efficiency was calculated by $[(I_0/I)\text{-}1]$ where the I_0 and I are fluorescence intensities in the absence of presence of quencher, respectively. A linear relationship of $[(I_0/I)\text{-}1] = 0.0635\,[Mn^{7+}] - 0.2601$ was observed (inset of Fig. 6b) in a range of 0–100 μM with a good correlation coefficient (R^2 = 0.9943, $n = 3$).

The calculated limit of detection (LOD) was 46.8 nM in which LOD = 3δ/s, where δ is the standard deviation of ten blank samples and s is the slope of the linear relationship. According to the US EPA guidelines, the recommended short term exposure level of Mn^{7+} is 22.1 μM while the drinking water quality intended to control discoloration, staining and bitter metallic taste is maintained at 1.1 μM [18]. Since the LOD of the nanoprobe is significantly below these targeted levels, it was a promising candidate for the detection of Mn^{7+} in water samples.

To identify the sensing mechanism, further experiments were conducted. Generally, quenching of fluorescence in the presence of a quencher would occur due to either formation of non-radiative ground state complexation or by Förster resonance energy transfer (FRET) or the inner filter effect (IFE) or photoinduced electron transfer (PET) from N/Al-CD to Mn^{7+} [53]. There is considerable spectral overlay between the absorption spectra of Mn^{7+} and excitation spectra of N/Al-CDs (Fig. 7a) which indicated the possible involvement of the FRET or IFE mechanism. However, absorption spectrums of

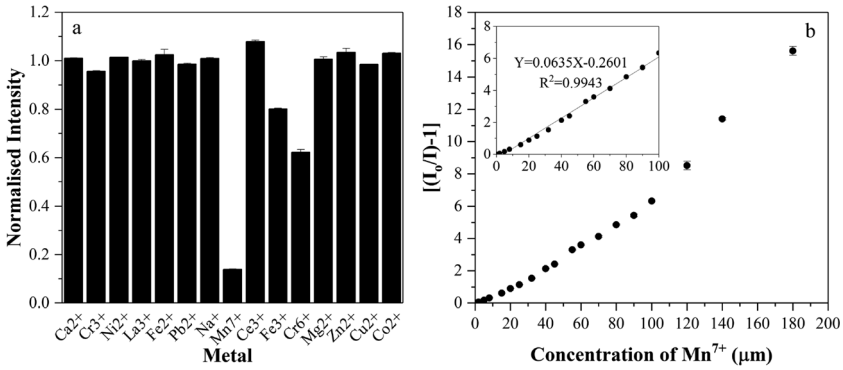

Fig. 6 **a** Selectivity of N/Al-CDs towards different metal ions, **b** Relationship between quenching efficiency against Mn^{7+} concentration

other metals with the excitation/emission spectrum shows the direct overlap of Cr^{6+} ion. It is concluded that this overlap by Cr^{6+} was responsible for the quenching of ~40% of CD fluorescence through IFE as reported by Tan et al. [54]. However, the overall quenching efficiency for Mn^{7+} was significantly higher compared to Cr^{6+}. This indicates the presence of another dominant mechanism. To ascertain if the quenching was induced by FRET, time-resolved fluorescence lifetime spectra (Fig. 7b) were studied. After fitting the spectra with a double-exponential function, the average decay time was measured to be 1.60 ns ($X^2 = 0.85$) and 1.68 ns ($X^2 = 0.87$) in the absence and the presence of the quencher Mn^{7+}, respectively. The almost identical decay times could reasonably eliminate the FRET mechanism. Figure 7c shows the UV-Vis spectra of N/Al-CDs, Metal, N/Al-CDs -Metal system and the sum absorption spectrum between N/Al-CDs and Metal for Mn^{7+}. It could be observed the CD-Mn^{7+} complex absorption spectrum did not superimpose with the sum of CD and Mn absorption spectra. CDs are a rich source of pi bonds and this is further confirmed by the strong peak corresponding to C=C

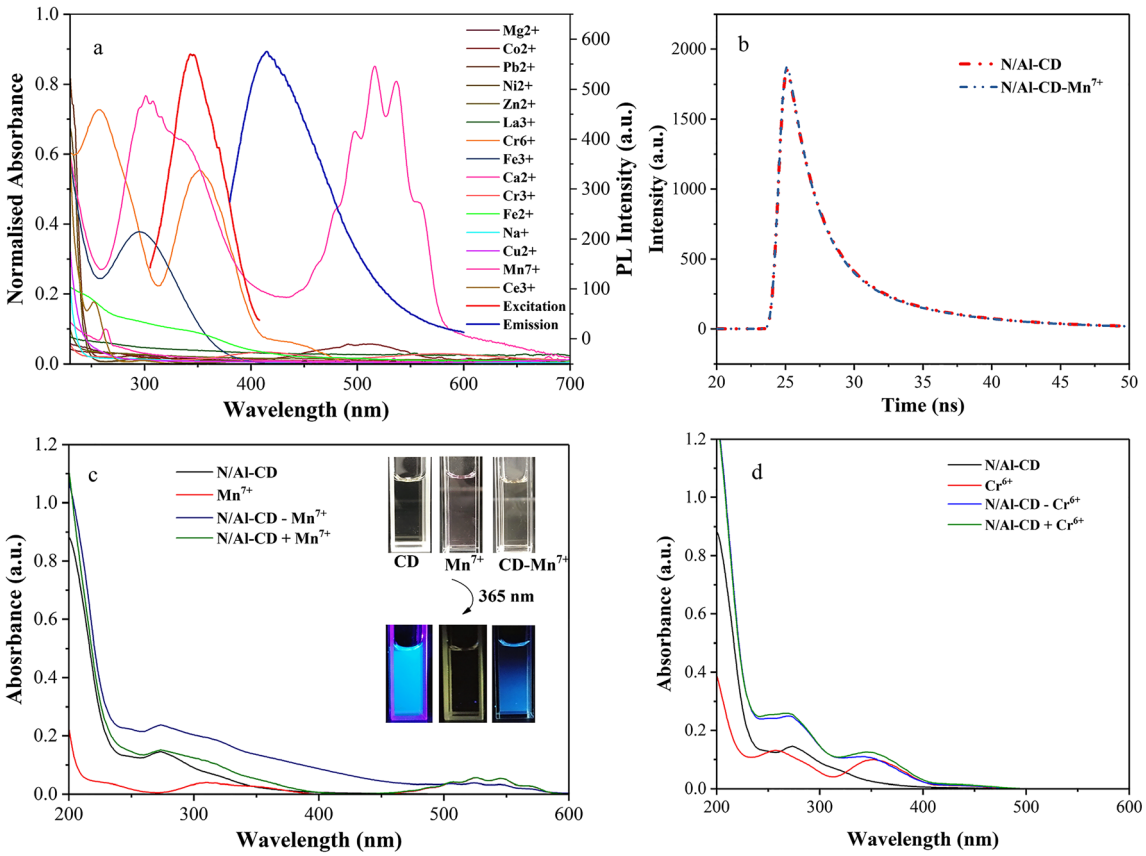

Fig. 7 **a** Normalised UV-Vis adsorption spectrums with metals and maximum excitation and emission spectrums of N/Al-CDs, **b** Time-correlated single-photon counting of N/Al-CDs in the presence and absence of Mn^{7+} (inset 7b) images of N/Al-CDs with quencher under white and UV ($\lambda_{ex} = 365$ nm) lights, **c** and **d** UV–visible spectra of N/Al-CDs, Metal, N/Al-CDs -Metal complex and sum of N/Al-CDs and metal absorption spectrums for Mn^{7+} and Cr^{6+} respectively

Table 1 Detection of Mn^{7+} in tap water and Jurong lake water samples ($n = 3$)

Sample	Spiked Concentration (μM)	Measured Concentration (μM)	Recovery %	RSD %
Lake Water	8.00	7.69	96.25	3.77
	15.00	14.14	94.26	3.86
	20.00	21.23	106.16	3.59
Tap Water	8.00	7.41	92.58	1.19
	15.00	15.88	105.84	0.98
	20.00	20.89	104.45	1.25

bond in the FTIR spectra. It is expected that Mn^{7+} coordinates with the alkenes and upon photoexcitation the excited state electrons undergo redox reaction by reducing Mn^{7+} to Mn^{4+} [55]. This was further confirmed by the visible colour change of the purple Mn^{7+} to brown Mn^{4+} upon the addition of CDs (Fig. 7c inset). However, CD- Cr^{6+} complex did not deviate from the sum of CD and Cr^{6+} absorption spectrum indicating the absence of electron transfer complex formation (Fig. 7d). Thus, the non-radiative PET oxidative transfer process has dominated the fluorescence quenching process.

To verify its sensitivity in practical applications, tap water from the Residuals and Resource Reclamation Centre (R3C) Laboratory and lake water from Jurong Lake were used. Lake water was filtered with a 0.45 μm filter followed with a 0.22 μm filter prior to testing. No Mn^{7+} in the original water samples was detected and the pH was 7.6 and 7.0 for lake water and tap water, respectively. All samples were spiked with a known amount of Mn^{7+} and the recovery percentage and relative standard deviation (RSD) were calculated as shown in Table 1.

In both water samples, good recovery percentages were shown with a range from 92.58%–106.16% with an RSD <3.9% for lake water and < 1.3% for tap water. These results further indicated the reliability and sensitivity of the synthesised N/Al-CDs sensor to detect Mn^{7+} in water samples.

Conclusion

Novel, highly fluorescent carbon dots with a quantum yield of 28.7% were successfully produced by co-doping a durian shell waste with nitrogen and aluminum in a facile one pot hydrothermal carbonisation process. The presence of aluminum and nitrogen on N/Al-CDs was confirmed with structural and microscopic analysis. The optical characterisation showed N/Al-CDs emitted blue fluorescence and the maximum emission was at 415 nm with an excitation wavelength of 345 nm. Durian shell waste is primarily cellulose and developing CDs with high quantum yield and excellent photostability provides new opportunities in the future developments of carbon quantum dots and resource recovery from waste. The resulting N/Al-CDs could be used as an efficient fluorescent sensor to detect Mn^{7+}. With high selectivity and a limit of detection at 46.8 nM, the synthesised N/Al-CDs were challenged with actual water systems wherein the CDs successfully determined the Mn^{7+} levels. Thus, this study presented an efficient and simple method for production of a cellulose based fluorescent nanoprobe Mn^{7+} detection in environmental water systems.

Acknowledgements The authors would like to thank the Interdisciplinary Graduate School of Nanyang Technological University and Nanyang Environment & Water Research Institute for the financial and technical support extended to this study. We would like to acknowledge Dr. Pan Chaozhi from Environmental Bio-innovations Group for the insights that improved the manuscript quality and finally the Facility for Analysis, Characterization, Testing and Simulation, Nanyang Technological University, Singapore, for use of their transmission electron microscopy facilities.

Compliance with Ethical Standards

Competing Interests The authors declare that they have no competing interests.

References

1. Rooj B et al. (2018) Green synthesized carbon quantum dots from polianthes tuberose L. Petals for Copper (II) and Iron (II) detection. Journal of fluorescence: p. 1–7
2. Bharathi D et al (2018) Green and cost effective synthesis of fluorescent carbon quantum dots for dopamine detection. J Fluoresc 28(2):573–579
3. Atchudan R et al (2018) Hydrothermal conversion of Magnolia liliiflora into nitrogen-doped carbon dots as an effective turn-off fluorescence sensing, multi-colour cell imaging and fluorescent ink. Colloids Surf B: Biointerfaces 169:321–328
4. Marinovic A et al (2017) Carbon-Nanodot solar cells from renewable precursors. ChemSusChem 10(5):1004–1013
5. Jayaweera S, Yin K and Ng WJ (2018) Nitrogen-doped durian shell derived carbon dots for inner filter effect mediated sensing of tetracycline and fluorescent ink. Journal of fluorescence: p. 1–9
6. Lu Y et al (2018) Facile hydrothermal synthesis of carbon dots (CDs) doped ZnFe 2 O 4/TiO 2 hybrid materials with high photocatalytic activity. J Photochem Photobiol A Chem 353:10–18
7. Wang F et al (2016) Fluorescence quenchometric method for determination of ferric ion using boron-doped carbon dots. Microchim Acta 183(1):273–279
8. Hola K et al (2014) Photoluminescence effects of graphitic core size and surface functional groups in carbon dots: COO− induced red-shift emission. Carbon 70:279–286

9. Dong Y et al (2013) Carbon-based dots co-doped with nitrogen and sulfur for high quantum yield and excitation-independent emission. Angew Chem 125(30):7954–7958
10. Yang Z et al (2014) Nitrogen-doped, carbon-rich, highly photoluminescent carbon dots from ammonium citrate. Nanoscale 6(3):1890–1895
11. Gong X et al (2015) Low temperature synthesis of phosphorous and nitrogen co-doped yellow fluorescent carbon dots for sensing and bioimaging. J Mater Chem B 3(33):6813–6819
12. Park Y et al (2016) Improving the functionality of carbon nanodots: doping and surface functionalization. J Mater Chem A 4(30): 11582–11603
13. Xu Q et al (2016) Facile synthesis of copper doped carbon dots and their application as a "turn-off" fluorescent probe in the detection of Fe 3+ ions. RSC Adv 6(34):28745–28750
14. Xu Q et al (2016) Highly fluorescent Zn-doped carbon dots as Fenton reaction-based bio-sensors: an integrative experimental–theoretical consideration. Nanoscale 8(41):17919–17927
15. Ma Y et al (2017) A ratiometric fluorescence universal platform based on N, cu codoped carbon dots to detect metabolites participating in H2O2-generation reactions. ACS Appl Mater Interfaces 9(38):33011–33019
16. Wang Y et al (2015) Functionalization of carbonaceous Nanodots from MnII-coordinating functional knots. Chem Eur J 21(42): 14843–14850
17. Lin L et al. (2018) Metal ions doped carbon quantum dots: Synthesis, physicochemical properties, and their applications. TrAC Trends in Analytical Chemistry
18. Willhite C et al (2013) Emergency do not consume/do not use concentrations for potassium permanganate in drinking water. Human & experimental toxicology 32(3):275–298
19. Devai I, Delaune R (2002) Effectiveness of selected chemicals for controlling emission of malodorous sulfur gases in sewage sludge. Environ Technol 23(3):319–329
20. Tucker CS (1984) Potassium permanganate demand of pond waters. The Progressive Fish-Culturist 46(1):24–28
21. Ohlweiler O, Schneider AM (1972) Standardization of potassium permanganate by titration of sodium oxalate in presence of perchloric acid and manganese (II) sulfate. Anal Chim Acta 58(2): 477–480
22. Adler SJ, Noyes RM (1955) The mechanism of the permanganate-oxalate reaction. J Am Chem Soc 77(8):2036–2042
23. Fowler RM, Bright H (1935) Standardization of permanganate solutions with sodium oxalate. J Res Natl Bur Stand 15:493–501
24. Sun X, Lei Y (2017) Fluorescent carbon dots and their sensing applications. TrAC Trends Anal Chem 89:163–180
25. Wang Y et al (2017) Fluorescent carbon dots: rational synthesis, tunable optical properties and analytical applications. RSC Adv 7(65):40973–40989
26. Jayaweera S et al. (2018) Facile preparation of fluorescent carbon dots for label-free detection of Fe3+. Journal of Photochemistry and Photobiology A: Chemistry
27. Yokel RA (1994) Aluminum chelation: chemistry, clinical, and experimental studies and the search for alternatives to desferrioxamine. Journal of Toxicology and Environmental Health, Part A Current Issues 41(2):131–174
28. Peng G et al (2015) Effect of carbon surface functional groups on the synthesis of Ru/C catalysts for supercritical water gasification. Catalysis Science & Technology 5(7):3658–3666
29. Shen L et al (2013) Growth and stabilization of silver nanoparticles on carbon dots and sensing application. Langmuir 29(52):16135–16140
30. Shi J et al (2017) Green synthesis of fluorescent carbon dots for sensitive detection of Fe 2+ and hydrogen peroxide. J Nanopart Res 19(6):209
31. Lu W et al (2012) Economical, green synthesis of fluorescent carbon nanoparticles and their use as probes for sensitive and selective detection of mercury (II) ions. Anal Chem 84(12):5351–5357
32. Yuan M et al (2015) One-step, green, and economic synthesis of water-soluble photoluminescent carbon dots by hydrothermal treatment of wheat straw, and their bio-applications in labeling, imaging, and sensing. Appl Surf Sci 355:1136–1144
33. Xu Y et al (2014) Carbon quantum dot stabilized gadolinium nanoprobe prepared via a one-pot hydrothermal approach for magnetic resonance and fluorescence dual-modality bioimaging. Anal Chem 86(24):12122–12129
34. Prasannan A, Imae T (2013) One-pot synthesis of fluorescent carbon dots from orange waste peels. Ind Eng Chem Res 52(44): 15673–15678
35. Mehta VN et al (2015) One-step hydrothermal approach to fabricate carbon dots from apple juice for imaging of mycobacterium and fungal cells. Sensors Actuators B Chem 213:434–443
36. Liu C et al (2012) Dechlorinating transformation of propachlor through nucleophilic substitution by dithionite on the surface of alumina. J Soils Sediments 12(5):724–733
37. Hsu P-C, Chang H-T (2012) Synthesis of high-quality carbon nanodots from hydrophilic compounds: role of functional groups. Chem Commun 48(33):3984–3986
38. Chung S et al (2018) Overcome mass transfer limitation of PEMFC cathode via incorporation of hydrophobic carbon nanostructure. ECS Trans 85(13):475–487
39. Ferrari AC, Basko DM (2013) Raman spectroscopy as a versatile tool for studying the properties of graphene. Nat Nanotechnol 8(4): 235
40. Sim LC et al (2018) Sugarcane juice derived carbon dot–graphitic carbon nitride composites for bisphenol a degradation under sunlight irradiation. Beilstein journal of nanotechnology 9(1):353–363
41. Ivnitski D et al (2008) Entrapment of enzymes and carbon nanotubes in biologically synthesized silica: glucose oxidase-catalyzed direct electron transfer. Small 4(3):357–364
42. Zhang H et al (2016) Fluorescence determination of nitrite in water using prawn-shell derived nitrogen-doped carbon nanodots as fluorophores. ACS Sensors 1(7):875–881
43. Manova D et al (1998) Investigation of dc-reactive magnetron-sputtered AlN thin films by electron microprobe analysis, X-ray photoelectron spectroscopy and polarised infra-red reflection. Surf Coat Technol 106(2–3):205–208
44. Schmiers H et al (1999) Change of chemical bonding of nitrogen of polymeric N-heterocyclic compounds during pyrolysis. Carbon 37(12):1965–1978
45. Chiu HT, Sukachonmakul T (2015) Surface modification of aluminum nitride and silicon oxycarbide for silicone rubber composites. Surface Modification of Nanoparticle and Natural Fiber Fillers: p. 171–190
46. Iatsunskyi I et al (2015) Structural and XPS characterization of ALD Al2O3 coated porous silicon. Vacuum 113:52–58
47. Wang C et al (2015) A hydrothermal route to water-stable luminescent carbon dots as nanosensors for pH and temperature. Carbon 82:87–95
48. Deka MJ, Chowdhury D (2017) Chiral carbon dots and their effect on the optical properties of photosensitizers. RSC Adv 7(84): 53057–53063
49. Ortega-Liebana M et al (2017) Uniform luminescent carbon nanodots prepared by rapid pyrolysis of organic precursors confined within nanoporous templating structures. Carbon 117:437–446
50. Xu X et al (2016) Enriching photoelectrons via three transition channels in amino-conjugated carbon quantum dots to boost photocatalytic hydrogen generation. ACS Appl Mater Interfaces 8(22): 14118–14124

51. Yu P et al (2012) Temperature-dependent fluorescence in carbon dots. J Phys Chem C 116(48):25552–25557
52. Du F et al (2014) Economical and green synthesis of bagasse-derived fluorescent carbon dots for biomedical applications. Nanotechnology 25(31):315702
53. Tanwar AS et al (2016) Inner filter effect based selective detection of nitroexplosive-picric acid in aqueous solution and solid support using conjugated polymer. Acs Sensors 1(8):1070–1077
54. Wang H et al (2018) Facile one-step synthesis of highly luminescent N-doped carbon dots as an efficient fluorescent probe for chromium (VI) detection based on the inner filter effect. New J Chem 42(5): 3729–3735
55. Lee DG, Chen T (1989) Oxidation of hydrocarbons. 18. Mechanism of the reaction between permanganate and carbon-carbon double bonds. J Am Chem Soc 111(19):7534–7538